ELSEVIER

Chemical Engineering Journal 141 (2008) 298–304

Chemical Engineering Journal

www.elsevier.com/locate/cej

Hydrogen production by steam reforming of liquefied natural gas (LNG) over mesoporous nickel–alumina xerogel catalysts: Effect of nickel content

Jeong Gil Seo [a], Min Hye Youn [a], Ho-In Lee [a], Jae Jeong Kim [a], Eunsun Yang [b], Jin Suk Chung [c], Pil Kim [d], In Kyu Song [a,*]

[a] *School of Chemical and Biological Engineering, Research Center for Energy Conversion and Storage, Seoul National University, Shinlim-dong, Kwanak-ku, Seoul 151-744, Republic of Korea*

[b] *Department of Chemical Engineering and Applied Chemistry, University of Toronto, 200 College Street, Toronto, ON M5S 3E5, Canada*

[c] *School of Chemical Engineering and Bioengineering, University of Ulsan, Ulsan 680-749, Republic of Korea*

[d] *School of Environmental and Chemical Engineering, Chonbuk National University, Jeonju, Chonbuk 561-756, Republic of Korea*

Received 28 July 2007; received in revised form 30 December 2007; accepted 2 January 2008

Abstract

Mesoporous nickel–alumina xerogel (*X*NiAl) catalysts with various nickel contents were prepared by a single-step sol–gel method for use in hydrogen production by steam reforming of liquefied natural gas (LNG). The effect of nickel content on the catalytic performance of *X*NiAl catalysts was investigated. Nickel species were finely dispersed in the *X*NiAl catalysts through the formation of Ni–O–Al composite structure. The *X*NiAl catalysts served as efficient catalysts in the hydrogen production by steam reforming of LNG. Both LNG conversion and H_2 composition in dry gas showed volcano-shaped curves with respect to nickel content. Thus, optimal nickel content was required for maximum catalytic performance. The performance of *X*NiAl catalysts in the steam reforming of LNG increased with increasing reducibility of the catalyst. Among the catalysts examined, the 30NiAl (30 wt% Ni) catalyst with the highest reducibility showed the best catalytic performance. The highest surface area and the largest pore volume of the 30NiAl (30 wt% Ni) catalyst were also partly responsible for its superior catalytic performance.

Keywords: Mesoporous nickel–alumina xerogel catalyst; Sol–gel method; Liquefied natural gas; Steam reforming; Hydrogen production

1. Introduction

Hydrogen has attracted much attention as an alternative energy source due to its clean, renewable, and non-polluting nature [1]. Technological advances in hydrogen utilization such as fuel cell make hydrogen more important as a new energy source. However, development of feasible production methods for hydrogen is necessary, because abundant hydrogen is not given to us in nature but should be produced from water or organic compounds [2]. A number of catalytic reforming technologies, such as steam reforming, partial oxidation, and auto-thermal reforming, have been extensively investigated for the large and small scale hydrogen production from various hydrocarbons [3–11]. Among the reforming technologies, steam reforming of methane has been recognized as a feasible route to produce hydrogen. Liquefied natural gas (LNG), which is abundant and mainly composed of methane, can serve as an alternate source for hydrogen production by steam reforming reaction. The extensive piping system for LNG in modern cities also makes LNG well suited as a hydrogen source for residential reformers in fuel cell applications.

Nickel-based catalysts have been widely studied as efficient catalysts for various reactions, such as hydrogenation of unsaturated hydrocarbons and reforming of hydrocarbons [12–16]. In particular, Ni/Al_2O_3 catalysts have been recognized as promising catalysts for steam reforming reactions due to their low cost and high catalytic activity [17–21]. The Ni/Al_2O_3 catalysts, however, require high reaction temperatures and excess amounts of steam to prevent sintering of nickel particles and deposition

* Corresponding author. Tel.: +82 2 880 9227; fax: +82 2 889 7415.
E-mail address: inksong@snu.ac.kr (I.K. Song).

1385-8947/$ – see front matter © 2008 Elsevier B.V. All rights reserved.
doi:10.1016/j.cej.2008.01.001

of carbon species on the catalyst surface in the stream reforming reactions [3,9,22].

The catalytic activity of Ni/Al_2O_3 is closely related to both nickel content and nickel dispersion, but these two factors have opposite effects on the catalytic activity. With increasing nickel content, for example, the catalytic activity of Ni/Al_2O_3 increases due to the increased number of active nickel sites, but the dispersion of nickel particles decreases due to the aggregation of nickel species. In general, nickel content of conventional Ni/Al_2O_3 catalysts used in the steam reforming reactions does not exceed 12 wt% to avoid severe aggregation or sintering of nickel particles during the reactions [23]. Although stable Ni/Al_2O_3 catalysts can be obtained by lowering the nickel content, they may show an inferior catalytic activity due to the insufficient number of active nickel sites. Furthermore, the nickel catalysts that are highly dispersed on Al_2O_3 readily form nickel aluminate phases through the incorporation of Ni^{2+} into the lattice of Al_2O_3 [21,24,25]. The strong metal–support interaction, in turn, inhibits the reduction of nickel aluminate into active metallic nickel.

Many attempts have been made to increase the stability of Ni/Al_2O_3 catalysts in the steam reforming reactions [17,20,21,26–28]. The performance of Ni/Al_2O_3 catalysts in the steam reforming reactions depends not only on the nature and structure of active nickel, but also on the chemical and physical properties of Al_2O_3. It is known that metal oxides prepared by a sol–gel method retain hydroxyl-rich surfaces, and therefore, exhibit unique chemical and physical properties compared to those prepared by a conventional method. In particular, alumina materials prepared by a sol–gel method have high-surface areas and controllable chemical and physical properties. It has been reported that a nickel–alumina xerogel catalyst prepared by a sol–gel method inhibited carbon deposition in the dry reforming of methane, resulting in the enhanced methane conversion and coke resistance [29,30]. Therefore, developing a sol–gel derived nickel–alumina catalyst, which retains both high activity and stability in the steam reforming of LNG, would be worthwhile.

In this work, a series of mesoporous nickel–alumina xerogel catalysts with various nickel contents were prepared by a single-step sol–gel method for use in hydrogen production by steam reforming of LNG. The effect of nickel content on the catalytic performance of mesoporous nickel–alumina xerogel catalysts was investigated. It is expected that the mesoporous nickel–alumina xerogel (*X*NiAl) catalysts prepared by a single-step sol–gel method would show a high and stable catalytic performance in the steam reforming of LNG without significant nickel sintering and carbon deposition.

2. Experimental

2.1. Preparation of mesoporous nickel–alumina xerogel catalysts

A series of mesoporous nickel–alumina xerogel catalysts with various nickel contents were prepared by a single-step sol–gel method, according to the similar method reported in the literatures [29–31]. A known amount of aluminum precursor (aluminum *sec*-butoxide, Sigma–Aldrich) was dissolved in ethanol at 80 °C with vigorous stirring. Small amounts of distilled water and nitric acid, which had been diluted with ethanol, were slowly added into the solution of aluminum precursor for the partial hydrolysis of the aluminum precursor. After maintaining the resulting solution at 80 °C for a few minutes, a clear sol was obtained. The sol was cooled to 60 °C, and then a known amount of nickel precursor (nickel acetate tetrahydrate, Sigma–Aldrich) was slowly added into the sol to obtain a nickel–alumina sol. After cooling the nickel–alumina sol to room temperature, a monolithic gel was obtained by adding an appropriate amount of water diluted with ethanol into the sol. The gel was aged for 7 days, and then dried overnight at 120 °C. The resulting powder was finally calcined at 700 °C for 5 h to yield the mesoporous nickel–alumina xerogel catalyst. The prepared nickel–alumina xerogel catalysts were denoted as *X*NiAl ($X = 15$, 20, 25, 30, 35, and 40), where X represents the nickel content (wt%) in the catalyst. For example, 30NiAl denotes a 30-wt% nickel–alumina xerogel catalyst.

For the purpose of comparison, a nickel catalyst supported on commercial Al_2O_3 (Degussa) was prepared by an impregnation method. The nickel loading was fixed at 20 wt%. The supported nickel catalyst was denoted as $20Ni/Al_2O_3$-impregnation.

2.2. Characterization

Nitrogen adsorption–desorption isotherms of the catalysts were obtained with an ASAP-2010 (Micromeritics) instrument. Average pore diameters of the catalysts were determined by the Barret–Joyner–Hallender (BJH) method applied to the desorption branch of the nitrogen isotherm. Nickel dispersion on the catalysts was examined by TEM analyses (Jeol, JEM-2000EXII). Crystalline phases of the catalysts were investigated by XRD (MAC Science, M18XHF-SRA) measurements using Cu Kα radiation ($\lambda = 1.54056$ Å) operated at 50 kV and 100 mA. In order to examine the reducibility of the catalysts, temperature-programmed reduction (TPR) measurements were carried out in a conventional flow system with a moisture trap connected to a thermal conductivity detector (TCD) at temperatures ranging from room temperature to 1000 °C with a ramping rate of 5 °C/min. For the TPR measurements, a mixed stream of H_2 (2 ml/min) and N_2 (20 ml/min) was used for 0.2 g of catalyst sample.

2.3. Steam reforming of LNG

Steam reforming of LNG was carried out in a continuous flow fixed-bed reactor at atmospheric pressure. Each calcined catalyst (100 mg) was charged into a tubular quartz reactor, and then reduced with a mixed stream of H_2 (3 ml/min) and N_2 (30 ml/min) at 700 °C for 3 h. Water was sufficiently vaporized and continuously fed into the reactor together with LNG (92.0 vol.% CH_4 and 8.0 vol.% C_2H_6) and N_2 carrier (30 ml/min). The steam/carbon ratio in the feed stream was fixed at 2.0, and the total feed rate with respect to the catalyst was maintained at 27,000 ml h^{-1}/g. The catalytic reaction was carried out at 600 °C. Reaction products were periodically sampled

and analysed using an on-line gas chromatograph (Younglin, ACME 6000) equipped with a thermal conductivity detector. LNG conversion and H_2 composition in dry gas were calculated on the basis of carbon balance as follows

$$\text{LNG conversion } (\%) = \left(1 - \frac{F_{CH_4,out} + F_{C_2H_6,out}}{F_{CH_4,in} + F_{C_2H_6,in}}\right) \times 100 \quad (1)$$

$$H_2 \text{ composition in dry gas } (\%) = \frac{F_{H_2,out}}{F_{H_2,out} + F_{CH_4,out} + F_{C_2H_6,out} + F_{CO,out} + F_{CO_2,out}} \times 100 \quad (2)$$

3. Results and discussion

3.1. Chemical and physical property of XNiAl catalysts

Physical properties of *X*NiAl (*X* = 15, 20, 25, 30, 35, and 40) catalysts were examined by nitrogen adsorption–desorption isotherm measurements. Fig. 1 shows the nitrogen adsorption–desorption isotherms and pore size distributions of selected *X*NiAl (*X* = 15, 30, and 40) catalysts. The *X*NiAl (*X* = 15, 30, and 40) catalysts showed IV-type isotherms with H_2-type hysteresis loops, indicating the existence of well-developed framework mesopores. Furthermore, the *X*NiAl (*X* = 15, 30, and 40) catalysts showed narrow pore size distributions centered at around 2–5 nm. The *X*NiAl (*X* = 20, 25, and 35) catalysts also showed isotherms, hysteresis loops, and pore size distributions similar to those observed for *X*NiAl (*X* = 15, 30, and 40) catalysts. These results indicate that mesoporous nickel–alumina xerogel catalysts were successfully prepared in this work.

Detailed chemical and physical properties of *X*NiAl (*X* = 15, 20, 25, 30, 35, and 40) catalysts are summarized in Table 1. For comparison, the physical properties of bare alumina xerogel [31] are also listed in Table 1. It was revealed that the nickel contents of *X*NiAl (*X* = 15, 20, 25, 30, 35, and 40) catalysts were almost identical to the target nickel loadings. The incorporation of nickel into mesoporous alumina did not greatly affect the surface area, but decreased the pore volume and average pore diameter of *X*NiAl (*X* = 15, 20, 25, 30, 35, and 40) catalysts, when compared to the bare alumina xerogel. It was found that the surface area and the pore volume of the catalysts showed volcano-shaped curves with respect to nickel content, although they did not show the same trend. Among the prepared catalysts, the 30NiAl catalyst exhibited the highest surface area and the largest pore volume.

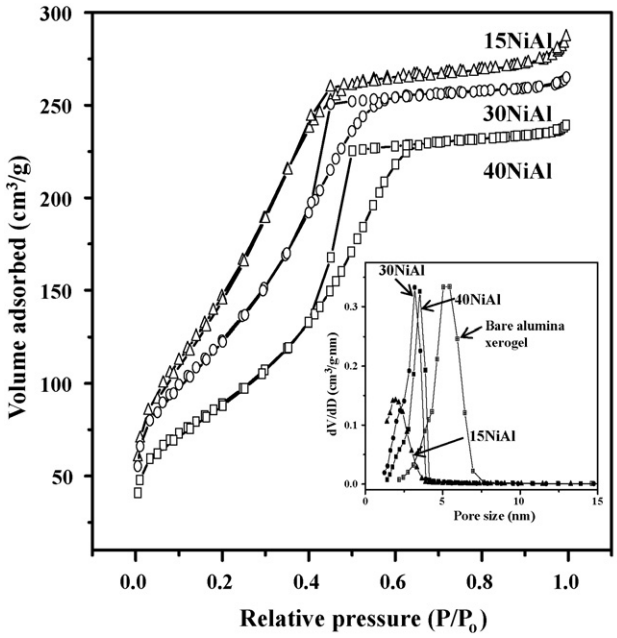

Fig. 1. Nitrogen adsorption–desorption isotherms and pore size distributions of selected *X*NiAl (*X* = 15, 30, and 40) catalysts. All the catalysts were calcined at 700 °C prior to the measurements.

3.2. Nickel dispersion

Fig. 2 shows the XRD patterns of *X*NiAl (*X* = 15, 20, 25, 30, 35, and 40) catalysts calcined at 700 °C for 5 h. For comparison, the XRD pattern of bare alumina xerogel [31] is also presented in Fig. 2. It is noteworthy that no diffraction peaks corresponding to nickel oxide were observed even in the 40NiAl

Table 1
Chemical and physical properties of *X*NiAl (*X* = 15, 20, 25, 30, 35, and 40) catalysts calcined at 700 °C for 5 h

Catalyst	Ni/Al atomic ratio[a]	Actual Ni loading (wt%)[a]	Surface area ($m^2\ g^{-1}$)[b]	Pore volume ($cm^3\ g^{-1}$)[c]	Average pore diameter (nm)[d]
Bare alumina xerogel	0.0	–	365	0.64	4.7
15NiAl	0.39	17.1 (15)	340	0.20	2.1
20NiAl	0.52	21.7 (20)	360	0.30	2.1
25NiAl	0.64	25.2 (25)	412	0.32	2.4
30NiAl	0.81	30.0 (30)	458	0.42	2.6
35NiAl	0.97	33.9 (35)	333	0.37	3.1
40NiAl	1.14	37.7 (40)	328	0.36	3.0

[a] Determined by ICP-AES analysis (values in parentheses represent the target nickel loading).
[b] Calculated by the BET equation.
[c] BJH desorption pore volume.
[d] BJH desorption average pore diameter.

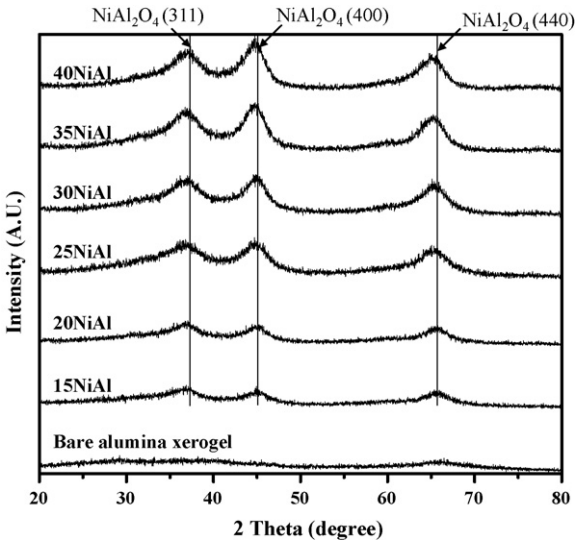

Fig. 2. XRD patterns of *X*NiAl (*X* = 15, 20, 25, 30, 35, and 40) catalysts calcined at 700 °C for 5 h.

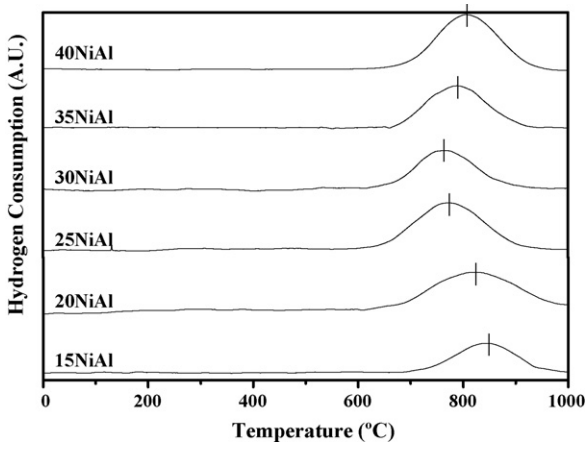

Fig. 4. TPR profiles of *X*NiAl (*X* = 15, 20, 25, 30, 35, and 40) catalysts calcined at 700 °C for 5 h.

catalyst. This result indicates that nickel species were finely dispersed in the *X*NiAl (*X* = 15, 20, 25, 30, 35, and 40) catalysts, resulting in the formation of small nickel particles that were under the detection limit of XRD measurement [32,33]. Instead, the diffraction peaks (solid lines) indicative of spinel nickel aluminate phase were observed in all the *X*NiAl (*X* = 15, 20, 25, 30, 35, and 40) catalysts. It was difficult to distinguish alumina phase from nickel aluminate phase due to the overlap of XRD peaks. The formation of nickel aluminate phase caused the lattice expansion of alumina because the ionic radius of Ni is larger than that of Al. In this work, it was observed that the (4 4 0) diffraction peak of alumina shifted to lower angle with increasing nickel content. The above result implies that a nickel aluminate phase was formed in the *X*NiAl (*X* = 15, 20, 25, 30, 35, and 40) catalysts due to the homogeneous mixing and interaction between alumina sol and nickel precursor during the catalyst preparation. It is likely that the anionic acetate groups in the nickel precursor (nickel acetate tetrahydrate) acted as chelating agents retarding hydrolysis and condensation of the alumina sol, which resulted in the formation of Ni–O–Al composite structure [30].

Fine dispersion of nickel species in the prepared catalysts was further confirmed by TEM analyses. Fig. 3 shows the TEM images of 30NiAl and 40NiAl catalysts calcined at 700 °C for 5 h. No visible evidence representing nickel agglomerates was found in both catalysts. This result indicates that nickel species were finely dispersed in the nickel–alumina xerogel catalysts, as confirmed by XRD measurements (Fig. 2). TEM images also showed that both 30NiAl and 40NiAl catalysts retained well-developed mesopores, as demonstrated in Fig. 1 and Table 1.

3.3. Reducibility

TPR measurements were carried out to investigate the reducibility of *X*NiAl (*X* = 15, 20, 25, 30, 35, and 40) cata-

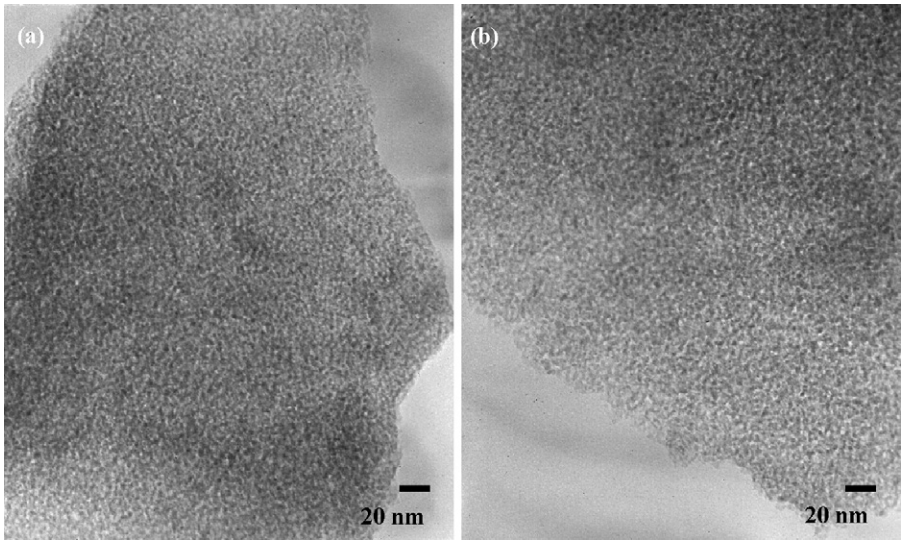

Fig. 3. TEM images of (a) 30NiAl and (b) 40NiAl catalysts calcined at 700 °C for 5 h.

Table 2
Catalytic performance of *X*NiAl (*X* = 15, 20, 25, 30, 35, and 40) and Ni/Al_2O_3-impregnation catalysts in the steam reforming of LNG at 600 °C

Catalyst	LNG conversion (%)[a]	H_2 composition in dry gas (%)[a]	CO composition in dry gas (%)[a]	CO_2 composition in dry gas (%)[a]	H_2/CO ratio[a]	Carbon deposition (wt%)[b]
Equilibrium at 600 °C	99.89	76.08	16.98	6.28	4.48	–
20Ni/Al_2O_3-impregnation	15.42	43.98	8.32	9.61	5.29	12.0
15NiAl	66.59	65.23	11.67	15.00	5.58	0.1
20NiAl	72.54	66.07	12.14	14.46	5.44	0.4
25NiAl	79.70	67.45	12.89	14.41	5.22	0.5
30NiAl	80.68	67.70	12.09	15.06	5.60	0.3
35NiAl	78.38	67.24	12.44	14.49	5.40	0.5
40NiAl	76.28	66.52	12.75	14.49	5.22	0.2

[a] Obtained after a 400-min reaction at 600 °C.
[b] Determined by CHNS elemental analysis after a 1000-min reaction at 600 °C.

lysts, and to examine the interaction between nickel species and alumina. Fig. 4 shows the TPR profiles of *X*NiAl (*X* = 15, 20, 25, 30, 35, and 40) catalysts. All *X*NiAl (*X* = 15, 20, 25, 30, 35, and 40) catalysts showed a broad reduction band at around 800 °C. This means that the stable nickel aluminate phase was formed in the *X*NiAl (*X* = 15, 20, 25, 30, 35, and 40) catalysts, in good agreement with the XRD results (Fig. 2). However, the reduction peak shifted to a lower temperature with increasing nickel content in the *X*NiAl (*X* = 15, 20, 25, and 30) catalysts. In other words, the interaction between nickel species and alumina decreased with increasing nickel content in the *X*NiAl (*X* = 15, 20, 25, and 30) catalysts. It is believed that the surface nickel aluminate phase, which is easier to be reduced than the bulk nickel aluminate phase, was preferentially formed with increasing nickel content in the *X*NiAl (*X* = 15, 20, 25, and 30) catalysts [34,35]. On the other hand, both 35NiAl and 40NiAl catalysts exhibited a higher reduction peak temperature than the 30NiAl catalyst. It was reported that the reducibility of nickel catalyst supported on alumina decreased with decreasing nickel loading and with increasing calcination temperature [36]. In the 35NiAl and 40NiAl catalysts, however, the reducibility decreased with increasing nickel content. It is believed that the bulk nickel aluminate phase was dominantly formed in the 35NiAl and 40NiAl catalysts unlike in the *X*NiAl (*X* = 15, 20, 25, and 30) catalysts. The nickel species mainly exist on the surface of alumina in the nickel catalyst impregnated on alumina. In the *X*NiAl (*X* = 15, 20, 25, 30, 35, and 40) catalysts, however, the nickel species exist both on the surface and in the bulk of alumina due to homogeneous mixing of nickel precursor and alumina sol, resulting in the formation of both surface nickel aluminate phase and bulk nickel aluminate phase. It is believed that the majority of nickel species was located in the bulk of alumina when the excess amount of Ni was added into alumina sol as the case of 35NiAl and 40NiAl catalysts. The TPR results presented in Fig. 4 clearly demonstrate that the reduction peak temperature of *X*NiAl (*X* = 15, 20, 25, 30, 35, and 40) catalysts showed a volcano-shaped curve with respect to nickel content. This means that optimal nickel content was required for the effective formation of surface nickel aluminate phase in the *X*NiAl (*X* = 15, 20, 25, 30, 35, and 40) catalysts. Among the catalysts examined, the 30NiAl catalyst showed the highest reducibility (the lowest reduction peak temperature).

3.4. Steam reforming of LNG

The catalytic performance of *X*NiAl (*X* = 15, 20, 25, 30, 35, and 40) and Ni/Al_2O_3-impregnation catalysts in the steam reforming of LNG at 600 °C is summarized in Table 2. It is well known that the steam reforming of methane is an equilibrium-controlled reaction. The equilibrium methane conversion and hydrogen composition in dry gas at 600 °C were 99.89 and 76.08%, respectively. The performance of *X*NiAl (*X* = 15, 20, 25, 30, 35, and 40) and 20Ni/Al_2O_3-impregnation catalysts was lower than the equilibrium value. However, the H_2/CO ratio was higher than the theoretical value.

Fig. 5 shows the LNG conversions with time on stream over 20NiAl, 30NiAl, and 20Ni/Al_2O_3-impregnation catalysts in the steam reforming of LNG at 600 °C. It is noticeable that the 20Ni/Al_2O_3-impregnation catalyst experienced a severe catalyst deactivation due to the significant carbon deposition on the catalyst surface. CHNS elemental analyses revealed that the 20Ni/Al_2O_3-impregnation catalyst contained 12 wt% carbon species after a 1000-min reaction. However, both 20NiAl and 30NiAl catalysts showed a stable catalytic performance during the reaction, extending over 1000 min. It was also observed that the *X*NiAl (*X* = 15, 25, 35, and 40) catalysts exhibited a stable catalytic performance during the reaction (although their

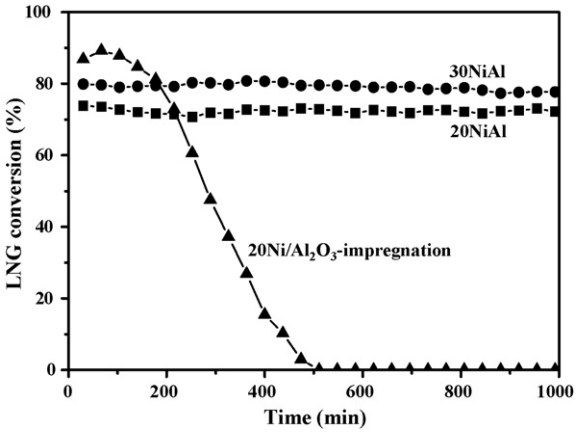

Fig. 5. LNG conversions with time on stream over 20NiAl, 30NiAl, and 20Ni/Al_2O_3-impregnation catalysts in the steam reforming of LNG at 600 °C. All catalysts were reduced at 700 °C prior to the reaction.

catalytic performance was not shown in Fig. 5). The amount of carbon species deposited on the *X*NiAl (*X* = 15, 20, 25, 30, 35, and 40) catalysts after a 1000-min reaction was less than 0.5 wt%.

The superior catalytic performance of the *X*NiAl (*X* = 15, 20, 25, 30, 35, and 40) catalysts compared to the 20Ni/Al_2O_3-impregnation catalyst can be explained by the chemical and physical properties of the *X*NiAl (*X* = 15, 20, 25, 30, 35, and 40) catalysts. It is believed that the highly dispersed nickel species and the well-developed mesopores in the *X*NiAl (*X* = 15, 20, 25, 30, 35, and 40) catalysts greatly enhanced coke resistance by preventing polymerization of the adsorbed surface hydrocarbons during the steam reforming reaction. Furthermore, the strong interaction between nickel species and alumina in the *X*NiAl (*X* = 15, 20, 25, 30, 35, and 40) catalysts effectively suppressed sintering of nickel particles through the formation of a stable nickel aluminate phase.

Fig. 6 shows the LNG conversions and H_2 compositions in dry gas over *X*NiAl (*X* = 15, 20, 25, 30, 35, and 40) catalysts in the steam reforming of LNG, plotted as a function of nickel content. Both LNG conversion and H_2 composition in dry gas showed volcano-shaped curves with respect to nickel content, and decreased in the order of 30NiAl > 25NiAl > 35NiAl > 40NiAl > 20NiAl > 15NiAl. This result indicates that optimal nickel content was required for maximum catalytic performance of mesoporous nickel–alumina xerogel catalysts. It is also believed that the highest surface area and the largest pore volume of 30NiAl catalyst were partly responsible for its superior catalytic activity (Table 1). The high surface area and large pore volume of the 30NiAl catalyst improved adsorption of both LNG and steam onto the catalyst surface. Harmonious adsorption of hydrocarbons (LNG) and steam onto the surface of the 30NiAl catalyst, in turn, enhanced the gasification reaction between two components. The surface nickel aluminate phase in the 30NiAl catalyst also played an important role in increasing the surface area of active nickel, resulting in the enhanced catalytic performance of the 30NiAl catalyst.

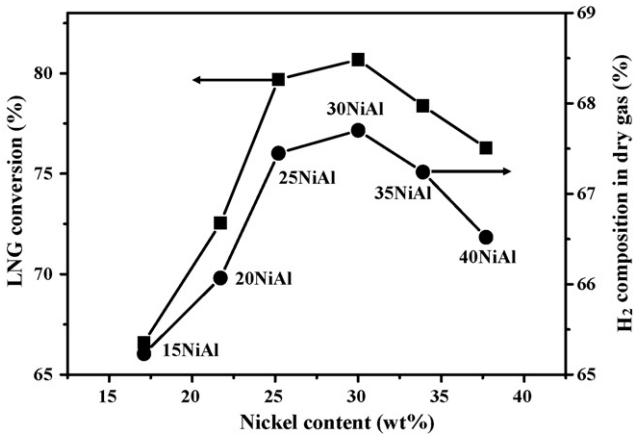

Fig. 6. LNG conversions and H_2 compositions in dry gas over *X*NiAl (*X* = 15, 20, 25, 30, 35, and 40) catalysts in the steam reforming of LNG, plotted as a function of nickel content. The catalytic reaction data were obtained at 600 °C after a 400-min reaction. All catalysts were reduced at 700 °C prior to the reaction.

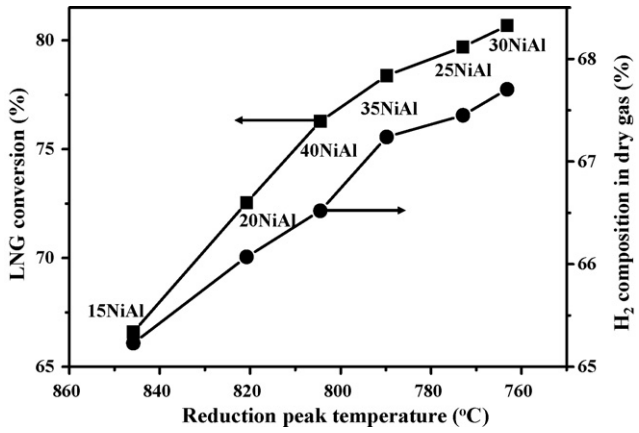

Fig. 7. Correlations between reducibility and catalytic activity of *X*NiAl (*X* = 15, 20, 25, 30, 35, and 40) catalysts in the steam reforming of LNG. The catalytic reaction data were obtained at 600 °C after a 400-min reaction.

3.5. Correlations between reducibility and catalytic activity

Although the reducibility of the catalyst is not the sole factor determining the catalytic performance in the steam reforming reaction, it can serve as a correlating parameter for the catalytic performance in the steam reforming reaction. Fig. 7 shows the correlations between reducibility (reduction peak temperature) and catalytic activity of *X*NiAl (*X* = 15, 20, 25, 30, 35, and 40) catalysts in the steam reforming of LNG. The reduction peak temperature determined by TPR measurements (Fig. 4) increased in the order of 30NiAl (763 °C) < 25NiAl (773 °C) < 35NiAl (790 °C) < 40NiAl (805 °C) < 20NiAl (821 °C) < 15NiAl (846 °C). The lower reduction peak temperature corresponds to the higher reducibility of the catalyst. It should be noted that both LNG conversion and H_2 composition in dry gas were well correlated with the reducibility of the catalyst. Both LNG conversion and H_2 composition in dry gas increased with increasing reducibility of the catalyst; more reducible catalyst showed a better catalytic performance in the steam reforming of LNG. It is believed that the surface area of metallic nickel was higher in the more reducible catalyst through the formation of surface nickel aluminate phase. Among the catalysts tested, the 30NiAl catalyst with the highest reducibility showed the best catalytic performance. Therefore, it is concluded that optimal nickel content was required for maximum catalytic performance of mesoporous nickel–alumina xerogel catalysts in the steam reforming of LNG.

4. Conclusions

A series of mesoporous nickel–alumina xerogel catalysts with various nickel contents were prepared by a single-step sol–gel method, and were applied to hydrogen production by steam reforming of LNG. The effect of nickel content on the catalytic performance of *X*NiAl (*X* = 15, 20, 25, 30, 35, and 40) catalysts was investigated. Physical properties of *X*NiAl (*X* = 15, 20, 25, 30, 35, and 40) catalysts were affected by nickel content. Nickel species were finely dispersed in the *X*NiAl (*X* = 15, 20,

25, 30, 35, and 40) catalysts through the formation of Ni–O–Al composite structure. The *X*NiAl (*X* = 15, 20, 25, 30, 35, and 40) catalysts showed a stable catalytic performance in the steam reforming of LNG. It was found that both LNG conversion and H_2 composition in dry gas showed volcano-shaped curves with respect to nickel content, and decreased in the order of 30NiAl > 25NiAl > 35NiAl > 40NiAl > 20NiAl > 15NiAl. It was also revealed that both LNG conversion and H_2 composition in dry gas increased with increasing reducibility of the catalyst. Among the catalysts tested, the 30NiAl catalyst with the highest reducibility showed the best catalytic performance. The highest surface area and the largest pore volume of the 30NiAl catalyst also played important roles in enhancing the gasification reaction between adsorbed hydrocarbons and steam. In conclusion, the mesoporous nickel–alumina xerogel catalysts prepared by a single-step sol–gel method served as efficient catalysts in the hydrogen production by steam reforming of LNG. In addition, optimal nickel content was required for maximum catalytic performance in the steam reforming of LNG.

Acknowledgements

The authors wish to acknowledge support from the Seoul Renewable Energy Research Consortium (Seoul R & BD Program) and RCECS (Research Center for Energy Conversion and Storage: R11-2002-102-00000-0).

References

[1] M. Schrope, Nature 414 (2001) 682–684.
[2] C.D. Blasi, G. Sinorelli, G. Portoricco, Ind. Eng. Chem. Res. 38 (1999) 2571–2581.
[3] J.R. Rostrup-Nielsen, J. Sehested, J.K. Nørskov, Adv. Catal. 47 (2002) 65–139.
[4] J.N. Armor, Appl. Catal. A 176 (1999) 159–176.
[5] A. Ishihara, E.W. Qian, I.N. Finahari, I.P. Sutrisna, T. Kabe, Fuel 84 (2005) 1462–1468.
[6] M. Nurunnabi, Y. Mukinakano, S. Kado, B. Li, K. Kunimori, K. Suzuki, K. Fujimoto, K. Tomishige, Appl. Catal. A 299 (2006) 145–156.
[7] J.K. Lee, D. Park, Korean J. Chem. Eng. 15 (1998) 658–662.
[8] K.D. Ko, J.K. Lee, D. Park, S.H. Shin, Korean J. Chem. Eng. 12 (1995) 478–480.
[9] J.R. Rostrup-Nielsen, Catal. Today 63 (2000) 159–164.
[10] J. Sehested, J.A.P. Gelten, I.N. Remediakis, H. Bengaard, J.K. Nørskov, J. Catal. 223 (2004) 432–443.
[11] S.W. Nahm, S.P. Youn, H.Y. Ha, S.-A. Hong, A.P. Maganyuk, Korean J. Chem. Eng. 17 (2000) 288–291.
[12] A. Louloudi, N. Papayannakos, Appl. Catal. A 204 (2000) 167–176.
[13] V. Tsipouriari, Z. Zhang, X.E. Verykios, J. Catal. 179 (1998) 283–291.
[14] R. Molina, G. Poncelet, J. Catal. 199 (2001) 162–170.
[15] Z. Pan, M. Dong, X. Meng, X. Zhang, X. Mu, B. Zong, Chem. Eng. Sci. 62 (2007) 2712–2717.
[16] S. Cavallaro, V. Childo, A. Vita, S. Freni, J. Power Sources 123 (2003) 10–16.
[17] L. Kępiński, B. Stasińska, T. Borowiecke, Carbon 38 (2000) 1845–1856.
[18] O. Yokota, Y. Oku, T. Sano, N. Hasegawa, J. Matsunami, M. Tsuji, Y. Tamaura, Int. J. Hydrogen Energy 25 (2000) 81–86.
[19] K.O. Christensen, D. Chen, R. Lødeng, A. Holmen, Appl. Catal. A 314 (2006) 9–22.
[20] T. Borowiecki, A. Gołębiowski, B. Stasińska, Appl. Catal. A 153 (1997) 141–156.
[21] J.G. Seo, M.H. Youn, I.K. Song, J. Mol. Catal. A 268 (2007) 9–14.
[22] A.C.S.C. Teixeira, R. Giudici, Chem. Eng. Sci. 56 (2001) 789–798.
[23] K. Kochloefl, in: G. Ertl, H. Knözinger, J. Weitkamp (Eds.), Handbook of Heterogeneous Catalysis, vol. 4, Wiley, New York, 1997, pp. 1819–1831.
[24] P. Kim, Y. Kim, H. Kim, I.K. Song, J. Yi, Appl. Catal. A 272 (2004) 157–166.
[25] E.D. Dimotakis, T.J. Pinnavaia, Inorg. Chem. 29 (1990) 2393–2394.
[26] T. Borowiecki, G. Wojciech, D. Andrzej, Appl. Catal. A 270 (2004) 27–36.
[27] J.S. Lisboa, D.C.R.M. Santos, F.B. Passos, F.B. Noronha, Catal. Today 101 (2005) 15–21.
[28] S. Natesakhawat, R.B. Watson, X. Wang, U.S. Ozkan, J. Catal. 234 (2005) 496–508.
[29] J.-H. Kim, D.J. Suh, T.-J. Park, K.-L. Kim, Appl. Catal. A 197 (2000) 191–200.
[30] D.J. Suh, T.-J. Park, J.-H. Kim, K.-L. Kim, J. Non-Cryst. Solids 225 (1998) 168–172.
[31] J.G. Seo, M.H. Youn, K.M. Cho, S. Park, I.K. Song, J. Power Sources 173 (2007) 943–949.
[32] T. Ueckert, R. Lamber, N.I. Jaeger, U. Schubert, Appl. Catal. A 155 (1997) 75–85.
[33] G. Li, L. Hu, J.M. Hill, Appl. Catal. A 301 (2006) 16–24.
[34] M.L. Jacono, M. Schiavello, A. Cimino, J. Phys. Chem. 75 (1971) 1044–1050.
[35] A.N. Kharat, P. Pendleton, A. Badalyan, M. Abedini, M.M. Amini, J. Catal. 205 (2002) 7–15.
[36] M. Wu, D.M. Hercules, J. Phys. Chem. 83 (1979) 2003–2008.